COMPUTER-AIDED DESIGN & APPLICATIONS, 2016
VOL. 13, NO. 5, 693–700
http://dx.doi.org/10.1080/16864360.2016.1150716

Measuring mean cup depth in the optic nerve head

John K. Johnstone[1,2], Lindsay Rhodes[2], Massimo Fazio[2], Brandon Smith[2], Lan Wang[2], J. Crawford Downs[2], Cynthia Owsley[2] and Christopher A. Girkin[2]

[1]Department of Computer and Information Sciences, UAB, USA; [2]Department of Ophthalmology, UAB, USA

ABSTRACT
Since the deformation of structures in the optic nerve head (ONH) is associated with glaucoma and other diseases of the optic nerve, measurement of this deformation is of current research interest. This paper considers the computation of cup depth, a measurement of the depth of the internal limiting membrane (ILM). The computation of cup depth requires a reference structure against which to measure the ILM, and the construction of two reference structures is discussed, one based on Bruch's membrane opening (BMO) and the other based on the anterior surface of the peripapillary sclera (AS). A main focus of the paper is the robust computation of mean cup depth, which requires a good sampling of a reconstruction of the ILM surface. To evaluate our algorithm, the construction of synthetic datasets is considered.

KEYWORDS
Morphometry; cup depth; reference structure; meshing; sampling; computing the mean

1. Introduction

Structural changes in the optic nerve head (ONH) have been associated with the development of glaucomatous optic neuropathy – in particular, expansion of the optic cup due to loss of neuroretinal tissues and remodeling of the underlying lamina cribrosa – motivating a quantitative analysis of ONH morphology. Cup depth is a useful measure that reflects the anatomical changes seen in glaucoma [13] and can be calculated based on the shape of the internal limiting membrane (ILM). This paper considers the computation of mean cup depth. Unlike previous studies that have computed cup depth directly from images [14], from few samples [12], or that assess cup depth qualitatively rather than quantitatively [8], we build a full shape model of the ILM from dense point clouds. We also use algorithms from shape modeling to build reference structures and to measure cup depth, as opposed to using manual measurements.

A main focus of this paper is an algorithm for the robust computation of mean cup depth, an important and computationally interesting measurement. After describing the structure of an ONH dataset, we discuss the three major components of a computation of mean cup depth: computation of a reference structure, reconstruction of the underlying ILM surface, and sampling of cup depth across this surface. We consider two candidates for reference structure, one based on Bruch's membrane and the other on the sclera. The paper ends with a discussion of the construction of synthetic ONH datasets for evaluation of our algorithm.

2. ONH Dataset

The ONH is modeled from an ONH dataset, which has a unique structure: a collection of independent point clouds, each organized into radial planar sections sharing a rotational axis (Fig. 2 and 6). This is in contrast to the usual structure of point clouds in shape modeling: either unorganized points or point clouds organized into parallel sections (as in CT/MR imaging, topographical maps, and 3D printing). A radial slicing is natural for the optic nerve head, since the locus of interest is near the center of the volume, where radial slices concentrate the data. The radial sections are manually segmented (Fig. 1) from spectral domain optical coherence tomography (SDOCT) images by trained observers (Smith and Wang) [2], yielding a separate point cloud for each category of interest in the ONH. For the computation of Bruch cup depth, the categories of interest are the ILM (red in Fig. 2 and 3) and Bruch's membrane (BM) (blue in Fig. 2 and 3). For the computation of scleral cup depth, the categories of interest are the ILM and the anterior surface of the peripapillary sclera (AS) (magenta in Fig. 2 and 4).

CONTACT John Johnstone jkj@uab.edu

© 2016 CAD Solutions, LLC, http://www.cadanda.com

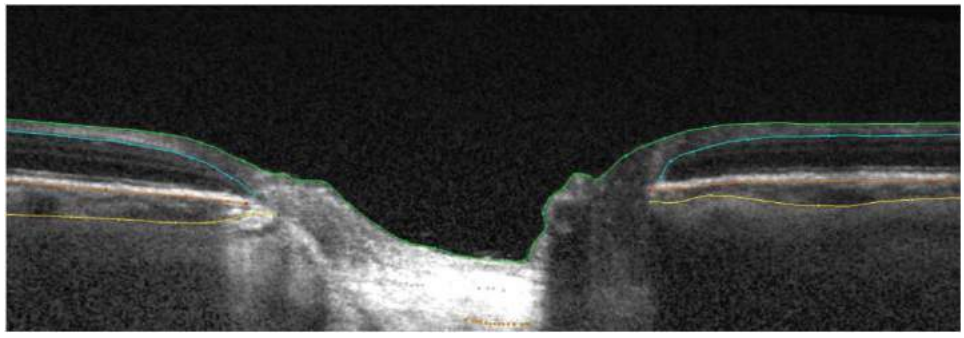

Figure 1. An SDOCT image and its manual segmentation. An ONH dataset is built from a series of these images.

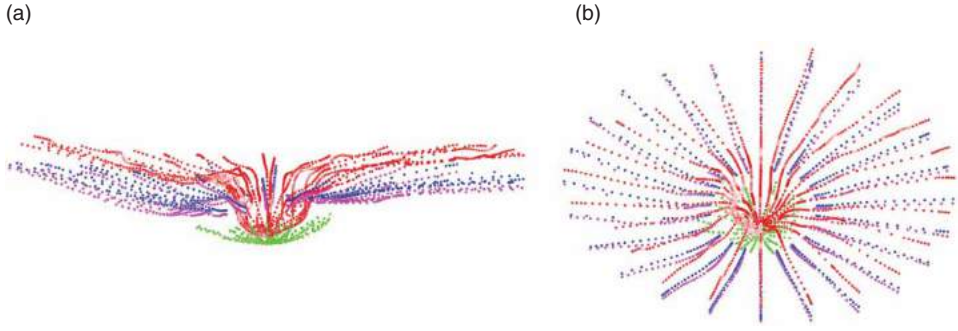

Figure 2. The ONH dataset. (a) The ILM (red), BM (blue), AS (magenta), and LC (green) point clouds of a typical ONH dataset. (b) A different viewpoint of this dataset, showing its organization into radial sections.

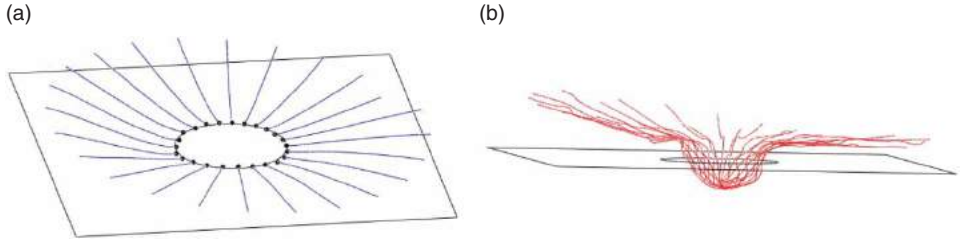

Figure 3. The Bruch reference structure. (a) BM (blue), BMO (black points), the BMO plane (the best-fitting plane of the BMO point cloud), and the BMO ellipse (the best-fitting ellipse of the BMO point cloud), which lies in the BMO plane. (b) The ILM (red), BMO plane, and BMO ellipse. The Bruch cup depth of a point of the ILM is its signed distance from this BMO plane, with positive distances on the laminar side (down in this image).

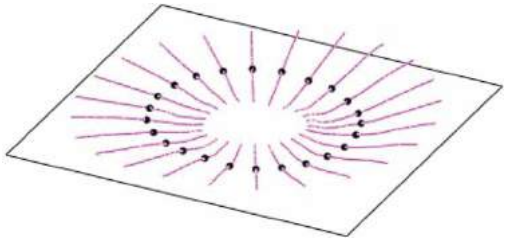

Figure 4. The scleral reference structure: AS (magenta), its scleral representatives (black points), and the scleral plane, their best-fitting plane.

The radial nature of an ONH dataset leads to some interesting challenges. In sampling for mean cup depth, care must be taken that sampling is not biased towards the center near the rotational axis. Due to the noise inherent in the segmentation, and misalignments of contiguous radial sections during the acquisition of the OCT scans, shape degeneracies can exist near the rotational axis, and an ONH dataset does not represent a manifold surface (the sections do not cross the axis at a common point). Fortunately, the topology of the ONH is simple and known, so the challenges are with geometry and not with topology.

3. Reference Structure

3.1. The Bruch Reference Structure

Cup depth is a measure of the depth of the ILM relative to the rest of the ONH. To measure this depth, a reference structure is necessary. The opening of Bruch's

membrane (BMO), the inner boundary of BM at the anterior end of the neural canal, is nearly planar and nearly elliptical, making it a good candidate for the basis of a reference structure (Fig. 3(a)). Consequently, a reference plane based on BM has been used in both clinical and histological studies to measure depth in the ONH (Fig. 3(b)). The *Bruch reference structure* (Fig. 3) consists of the best-fitting plane of the BMO (*BMO plane*), the best-fitting ellipse of the BMO (*BMO ellipse*), and the right elliptical cylinder defined by the best-fitting ellipse of the BMO (*BMO cylinder*). Note that the BMO ellipse lies in the BMO plane.

The *Bruch cup depth* of a point of the ILM is its signed distance from the BMO plane (Fig. 3(b)). Distance from the BMO plane is positive if and only if a point lies on the laminar side. The laminar side of the BMO plane is the halfspace that contains the lamina cribrosa (LC), a structure that always lies strictly on one side of the BMO plane (Fig. 2(a)). If the LC is not available in an ONH dataset, the laminar side may be defined instead by observing that each ILM section starts on the non-laminar side.

Measurement of cup depth should be constrained to the region over the ONH. The Bruch reference structure offers a natural mechanism to formalize this constraint: only ILM samples that lie within the BMO cylinder are considered during the computation of Bruch cup depth.

The computation of cup depth is simplified by working in a special coordinate frame. A *Bruch frame* is a coordinate frame whose origin is the center of the BMO ellipse, x-axis is the major axis of the BMO ellipse, z-axis is orthogonal to the BMO plane, and positive z-axis lies in the laminar half-space of the BMO plane. In a Bruch frame, the Bruch cup depth of an ILM point reduces to its z-coordinate. In a Bruch frame, filtering of the ILM against the BMO cylinder is also simplified, as the BMO cylinder acquires the normal form

$$\frac{x^2}{\alpha^2} + \frac{y^2}{\beta^2} = 1 \tag{3.1}$$

where α and β are the semi-axis lengths of the BMO ellipse. To move to a Bruch frame, first translate the center of the BMO ellipse to the origin, then rotate the BMO ellipse's major axis to the x-axis and the BMO plane's normal to the z-axis using the orthogonal matrix

$$\begin{pmatrix} E \\ E \times N \\ N \end{pmatrix} \tag{3.2}$$

where E is a unit vector in the direction of the BMO ellipse's major axis and N is the laminar-facing unit normal of the BMO plane.

The Bruch reference structure is computed using principal component analysis [3], as follows. Let $B = \{b_1, \ldots, b_n\}$ be the point cloud of the BMO, with mean $\bar{b}$ and covariance matrix

$$M = \frac{1}{n}\sum_{i=1}^{n}(b_i - \bar{b})(b_i - \bar{b})^t \tag{3.3}$$

The eigenvector $e_{\min}$ of M associated with the smallest eigenvalue defines the normal of the best-fitting plane of B (since it defines the direction of minimal variance of the point cloud). $\bar{b}$ is a point on the best-fitting plane. That is, the BMO plane is defined by $e_{\min}$ and $\bar{b}$. The eigenvector of M associated with the largest (resp., middle) eigenvalue defines the direction of the major (resp., minor) axis of the best-fitting ellipse. Eigenvectors may be computed robustly in C++ using the Eigen numerical library [5]. The BMO ellipse will be fully defined once its axis lengths and center are known. Note that the sample mean $\bar{b}$ is not the center of the BMO ellipse, since the point cloud is not uniformly sampled. However, since the BMO point cloud B lies close to its best-fitting ellipse, the axis lengths may be found by projecting B onto each principal axis and using the range of these points to define the axis length. The mean $\bar{b}$ is adjusted to the ellipse center by projecting it onto each principal axis, along with the extreme points on that axis, to determine how much $\bar{b}$ must be adjusted to lie midway on each axis.

3.2. The Scleral Reference Structure

As there is some concern and evidence [7] that BMO position may not be stable with increasing age, an alternative reference structure for cup depth may be defined using AS (Section 2). Basing a reference structure on AS, though less classical, may be more stable than basing it on BM [7]. An interior toroidal region of the sclera is used to define the best-fitting plane since the inner boundary of AS cannot be found reliably in all images. The scleral representative of an AS half-section (Fig. 4) is the mean of the samples that lie between 1700 and 1800 microns from the BMO cylinder's axis (using Euclidean distance). The band between 1700 and 1800 microns is used since it is most visible. Its mean is used as a smoothing operation. A scleral representative is not created on an AS half-section that does not intersect the entire 1700–1800-micron band. Before computation of the scleral representatives, it may be beneficial to resample the scleral half-sections (see Section 4 below). The *scleral plane* is the best-fitting plane of the scleral representatives of the AS half-sections (Fig. 4). Since the scleral representatives are close to planar, the computation of best-fitting plane is robust. Like the BMO plane, the best-fitting plane of the scleral representatives is computed using principal component analysis.

The *scleral reference structure* consists of the scleral plane and BMO cylinder. Only ILM samples that lie within the BMO cylinder are considered during the computation of scleral cup depth. The BMO cylinder is still used as the filtering cylinder, rather than a cylinder based on the best-fitting ellipse of the scleral representatives, since the BMO cylinder better reflects the neural canal.

The *scleral cup depth* of a point of the ILM is its signed distance from the scleral plane, positive if and only if the point lies on the laminar side. The sign of the distance is well defined, since the LC lies completely on one side of the scleral plane. If the LC is unavailable, the ILM can be used to define the sign, since the ILM always begins on the non-laminar side of the scleral plane.

The computation of scleral cup depth is simplified in a *scleral frame*: a coordinate frame whose z-axis is orthogonal to the scleral plane and positive z-axis lies in the laminar half-space of the scleral plane. In a scleral frame, the scleral cup depth of a point is its z-coordinate.

4. Meshing the ILM

Having shown how to compute cup depth at a point of the ILM, we now consider the computation of mean cup depth across the ILM. This requires a good sampling of cup depths. Since a sampling of the ILM surface requires a reconstruction of the ILM surface from the ILM sections (Fig. 5), we consider this first, then turn to the construction of a sampling in the next section.

A triangle mesh (Fig. 5) is built from the ILM sections using the contour reconstruction algorithm of Fuchs, Kedem and Uselton [4]. This algorithm uses minimal surface area as the guiding constraint, and reduces the minimization of area to the construction of a shortest path in a toroidal graph built from neighbouring sections.

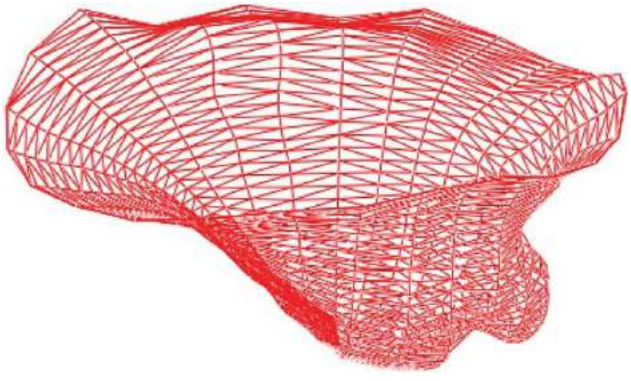

Figure 5. The ILM mesh: a minimal surface area reconstruction from a resampling of the ILM half-sections.

The ILM mesh may be constructed more efficiently and more robustly by using ILM half-sections rather than sections. Therefore, before meshing, each ILM section is split into two half-sections at the axis of rotation (AR) of the ONH dataset, the common axis of its radial sections (Fig. 6). A mesh is built between every pair of consecutive half-sections. Building the mesh between two half-sections, rather than two sections, has the advantage of enforcing the constraint that points on the AR should correspond. It is also more efficient, since the time complexity of the FKU algorithm is $O(2\,n^2 \log n)$ to mesh a pair of sections of size n, but

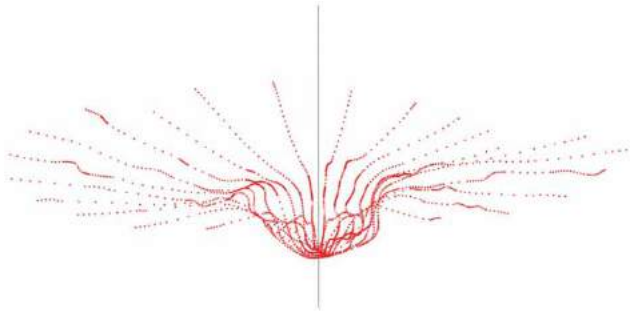

Figure 6. The axis of rotation (black) of an ONH dataset, shown along with the ILM (red).

$$O\left(4\left(\frac{n}{2}\right)^2 \log\left(\frac{n}{2}\right)\right) = O(n^2 \log n) \qquad (4.1)$$

to mesh two pairs of half-sections of size $\frac{n}{2}$.

The AR is computed by intersecting two ILM section planes, derived from the ILM section point clouds, taking care to use a robust pair of section planes (large angle, nonlinear triplet to define the plane). Then the point at which to split an ILM section may be found by walking along the section, looking for an AR crossing. In a coordinate frame whose z-axis is the AR, the AR is crossed as the coordinate (x or y) with the largest range changes sign, which is simpler than intersecting the AR with the section. After splitting an ILM section, the orientation of the second half-section is flipped so that all half-sections end at the axis, which is important for mesh construction.

To guarantee a good ILM mesh, the ILM half-sections should first be resampled. An ILM section may be oversampled in some areas and undersampled in others (Fig. 7(a)), prompting the construction of an interpolating curve, which can then be resampled at a uniform rate. Since the oversampled regions of the ILM section complicate the interpolation, the solution is to downsample (Fig. 7(b)), then interpolate, then upsample (Fig. 7(c)). Each ILM section is downsampled using a variant of Douglas-Peucker decimation [1]: while walking around the section, samples are removed whenever they preserve the invariant that every original sample is within a prescribed tolerance of the polygon defined by the

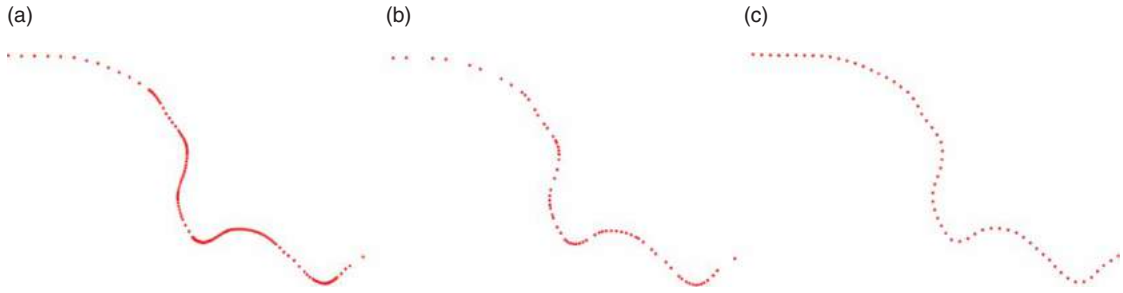

Figure 7. Resampling an ILM half-section. (a) The original ILM half-section. (b) Its downsampling. (c) Its uniform upsampling from an interpolating cubic B-spline.

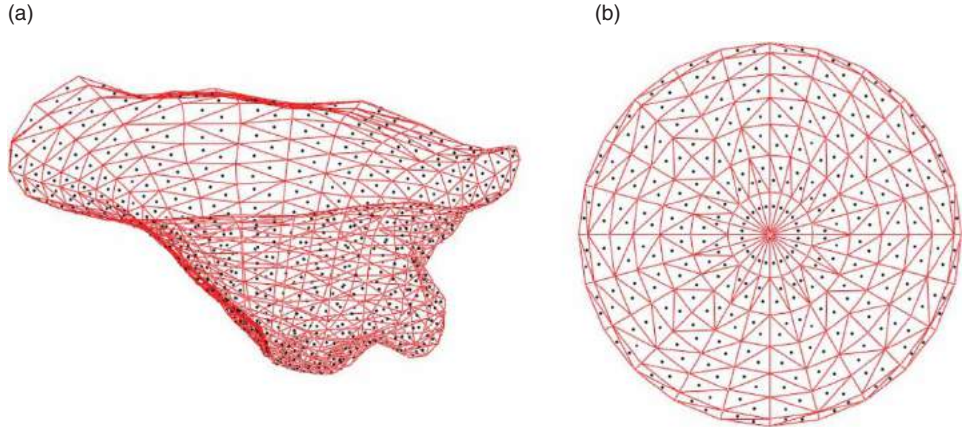

Figure 8. The centroid sampling. A sampling of the ILM mesh at triangle centroids, weighted by area, simulates a uniform sampling of the ILM surface. (a) A natural ONH dataset, using a sparse sampling for clarity. (b) Looking down at a synthetic paraboloid dataset (see Section 6), using a sparse sampling for clarity.

downsampling. A good choice of tolerance is .0001 of the radius of the ONH dataset's bounding box. The samples of the downsampled section are reliable for the construction of an interpolating cubic B-spline curve [10], which is then uniformly sampled for the desired robust sampling.

The last preparation for meshing is clipping. Since the domain of interest for cup depth is the BMO cylinder (Section 3.1), the ILM is clipped to the BMO cylinder, by clipping each ILM half-section to the BMO cylinder. Clipping is done after resampling. Clipping an ILM half-section to the BMO cylinder is similar to splitting an ILM section: walk along the half-section from the axis of rotation until the BMO cylinder is crossed, and clip at the intersection of this crossing segment with the cylinder (by solving a quadratic equation).

To recap, the ILM sections are first split into half-sections, then each ILM half-section is uniformly resampled, then each ILM half-section is clipped to the BMO cylinder. The ILM half-sections are now ready for the construction of a robust ILM mesh using the FKU contour reconstruction algorithm.

5. Approximating a uniform sampling of the ilm surface

A uniform sampling of the ILM surface (uniform in the space of the 2-manifold) is desirable for the computation of mean cup depth, yet a perfectly uniform sampling of the ILM is impossible. Two approaches were considered for building an approximately uniform sampling of the ILM surface. The first idea was to transfer a uniform sampling of parameter space to the mesh using a distortion-minimizing parameterization, as explored in texture mapping [6]. If a mesh is parameterized with minimal metric distortion, a uniform sampling of its parameter space will generate an approximately uniform sampling of the surface. Distortion-minimizing mesh parameterization has been studied extensively in the context of mapping an image to a mesh in texture mapping. Unfortunately, implementation of this technique revealed that, because of the complexity of the ILM geometry, too much metric distortion is introduced by the parameterization, leading to inferior results.

An alternate approach using weighting has proven successful. Mean cup depth is computed by sampling

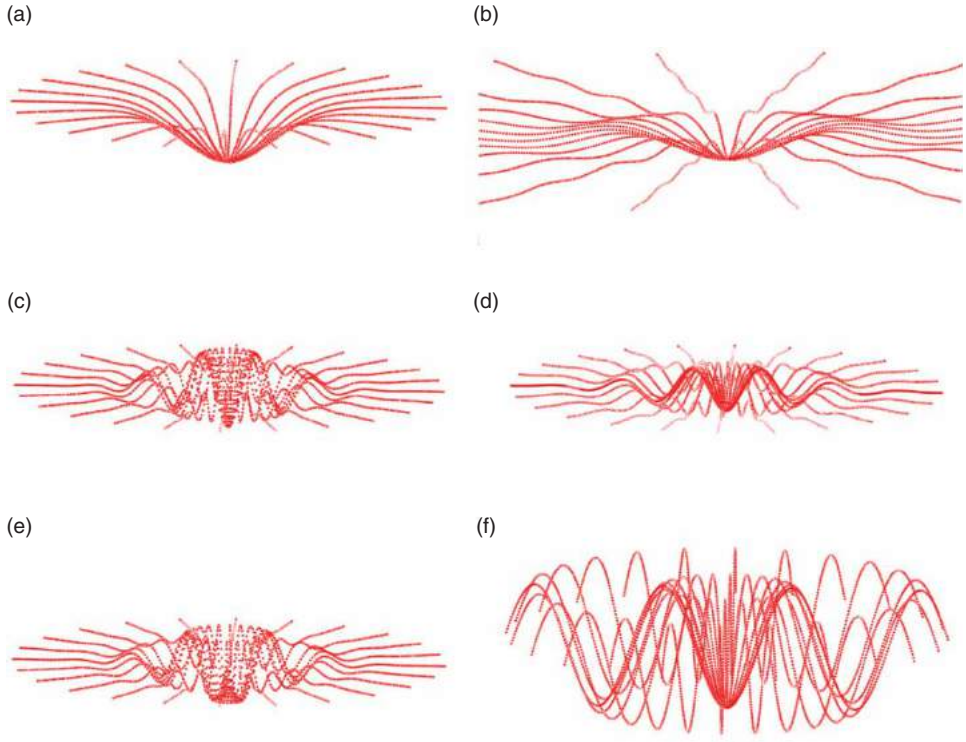

Figure 9. Synthetic ONH datasets were built to evaluate the accuracy of the algorithm. The ILM is generated from various mathematical functions that mirror the shape of the ILM, including the (a) Gaussian, (b) sinc, (c) even Gabor ($\sigma = .6$), (d) even Gabor ($\sigma = .8$) (e) odd Gabor, and (f) cosine.

cup depth at the triangle centroids of the ILM mesh and weighting by area. The observation is that the weighting of a non-uniform sampling can approximate a uniform sampling. The centroids of the ILM mesh triangles serve as the non-uniform sampling (Fig. 8), and the areas of the ILM mesh triangle as the weights. If the triangles of the clipped ILM mesh are $\{T_i\}$, the area of triangle T_i is A_i, the surface area of the entire clipped ILM mesh is A, and the cup depth of the centroid of T_i is c_i, then:

$$\text{mean cup depth} = \sum_i \frac{A_i}{A} c_i \tag{5.1}$$

The density of the centroid sampling can be controlled by the density of the mesh, which in turn can be controlled through the density of the resampling of each ILM section.

6. Synthetic datasets

An attractive way to evaluate the accuracy of our computation of mean cup depth is by running the algorithm on synthetic datasets for which the correct value can be computed analytically using integration. We consider the case of Bruch cup depth: scleral cup depth is completely analogous.

The first step is to build a synthetic ONH dataset that is amenable to integration. For Bruch cup depth, it is sufficient to build the ILM and BM. Various synthetic ILM surfaces were built by sampling mathematical functions that mirror the shape of the ILM: the Gaussian $z = G(x,\ y,\ \sigma) = \frac{1}{2\pi\sigma^2} e^{-\frac{x^2+y^2}{2\sigma^2}}$, even Gabor $z = \cos\left(\omega_0\sqrt{x^2+y^2}\right) G(x,\ y,\ \sigma)$, odd Gabor $z = \sin\left(\omega_0\sqrt{x^2+y^2}\right) G(x,\ y,\ \sigma)$, $\text{sinc}\, z = \frac{\sin\left(\sqrt{x^2+y^2}\right)}{\sqrt{x^2+y^2}}$, and cosine $z = \cos\left(w_0\sqrt{x^2+y^2}\right)$. Each was sampled in the 12 radial sections of an ONH dataset (Fig. 9).

The height and size of the BMO defines the domain of integration. The precise shape of the synthetic BM is arbitrary aside from the BMO that it defines. The BM is built so that the BMO plane and ellipse define a clean domain of integration for the ILM surface: a BMO plane orthogonal to the axis of rotation and a circular BMO ellipse centered on the analytic surface. The ILM must cover the BMO cylinder and be visible from the BMO plane (i.e., a ray fired orthogonal to the BMO plane will hit the surface at most once), since we want to relate our computation to a volume bounded by the ILM and the BMO plane. By varying the ILM surface and the size and height of the BMO ellipse, many different synthetic datasets may be built.

Table 1. Results on synthetic datasets using integration vs. our algorithm (with (5.1) replaced by (6.1)).

Function	σ	w_0	r	z	MATLAB integration	Our algorithm	% relative error
Gaussian	.7		1	−1	1.2036	1.20359	.00083%
Gaussian	.5		2	−1	1.0796	1.08042	.076%
even Gabor	.6	10	2	−.5	.4977	.497726	.0052%
even Gabor	.8	8	2	−.5	.4979	.498001	.020%
odd Gabor	.6	10	2	−.5	.4999	.49988	.0040%
Sinc			20	−2	2	2.00303	.15%
cosine		3	3	−2	2.0444	2.04409	.015%

We now make a small modification to our computation of mean cup depth, replacing Eqn. (5.1) with

$$\sum_i \left(\frac{A_i'}{A'}\right) c_i \tag{6.1}$$

where A_i' is the area of the projection of the triangle T_i onto the BMO plane (rather than the area of T_i) and $A' = \sum_i A_i'$. This new version of mean depth reduces to the ratio of a volume to an area: the volume of the ILM under the BMO plane divided by the area of the BMO ellipse. Therefore, this new computation can be compared against a numerical integration using MATLAB, since the ILM is a known mathematical surface. The volume integral is $\int_0^{2\pi} \int_0^{r'} \int_h^{f(\theta,r)} rdzdrd\theta$, where $f(\theta,\ r)$ is the ILM surface expressed in polar coordinates.

Tab. 1 compares the result from MATLAB integration with the result computed by our algorithm on a set of synthetic datasets. Along with varying the type of mathematical surface, the parameters of the ILM surface may be adjusted (the standard deviation σ of the underlying Gaussian or the frequency w_0 of the underlying cosine or sine) and the domain of integration may be adjusted (by changing the radius of the BMO cylinder and the height of the BMO plane, parameters r and z in Tab. 1). The percent relative error is also reported: the percent relative error of a computed solution x' from the true solution x is $\frac{100|x'-x|}{|x|}$. Note that our results are accurate to at least 3 decimal places with very low relative error.

Along with this evaluation against synthetic datasets, the components of the C++ code were rigorously tested. An alternative way to build synthetic datasets was also tested, by firing rays at an algebraic surface $f(x, y, z) = 0$.

7. Conclusions

The focus of this paper has been on the computational aspects of ONH morphometry. Our computation of cup depth has been used to analyze correlations between cup depth, race, and age [11]. This experience with the computation of mean cup depth has revealed the importance of cleaning the data, building a robust surface model for key anatomy, computing a robust reference structure, and using special reference frames during computation. The centrality of sampling is striking: a robust sampling of the ILM sections leads to a robust ILM mesh, which leads to a robust sampling of cup depths for mean depth.

The potential applications of shape modeling to the morphometry of anatomy are rich. The algorithms for mean cup depth in the optic nerve head developed in this paper are but one case study. In present and future work, we are considering a wider assortment of statistics for ONH morphometry, including volume, thickness, and curvature, and the alignment of a pair of ONH datasets for rigorous quantitative comparison.

Acknowledgements

This work was supported by the National Eye Institute [EY018926, EY14267, EY019869], the National Institute on Aging [R01AG04212], the EyeSight Foundation of Alabama, and Research to Prevent Blindness.

ORCID

John K. Johnstone http://orcid.org/0000-0003-4033-0066

References

[1] Ballard, D.; Brown, C.: Computer Vision, Prentice Hall, Englewood Cliffs, NJ, 1982.

[2] Downs, J.C.; Yang, H.; Girkin, C.; Sakata, L.; Bellezza, A.; Thompson, H.; Burgoyne, C.F.: Three-Dimensional Histomorphometry of the Normal and Early Glaucomatous Monkey Optic Nerve Head: Neural Canal and Subarachnoid Space Architecture, Investigative Ophthalmology and Visual Science, 48(7), 2007, 3195–3208. http://dx.doi.org/10.1167/iovs.07-0021

[3] Duda, R.O.; Hart, P.E.; Stork, D.G.: Pattern Classification, Wiley-Interscience, New York, 2001.

[4] Fuchs, H.; Kedem, Z.M.; Uselton, S.P.: Optimal Surface Reconstruction from Planar Contours, Communications of the ACM, 20(10), 1977, 693–702. http://dx.doi.org/10.1145/359842.359846

[5] Guennebaud, G.; Jacob, B.: Eigen v3, http://eigentuxfamily.org, 2010.

[6] Hormann, K.; Levy, B.; Sheffer, A.: Mesh Parameterization: Theory and Practice, SIGGRAPH Course Notes, 2007. http://www.inf.usi.ch/hormann/parameterization/

[7] Johnstone, J.; Fazio, M.; Rojananuangnit, K.; Smith, B.; Clark, M.; Downs, C.; Owsley, C.; Girard, M.J.A.; Mari,

J.M.; Girkin, C.A.: Variation of the Axial Location of Bruch's Membrane Opening with Age, Choroidal Thickness and Race, Investigative Ophthalmology and Visual Science, 55(3), 2014, 2004–2009. http://dx.doi.org/10.1167/iovs.13-12937

[8] Jonas, J.B.; Martus, P.; Budde, W.M.; Hayler, J.: Morphologic Predictive Factors for Development of Optic Disc Hemorrhages in Glaucoma, Investigative Ophthalmology and Visual Science, 43(9), 2002, 2956–2961. PMid:12202515

[9] Park, S.C.; De Moraes, C.G.; Teng, C.C.; Tello, C.; Liebmann, J.M.; Ritch, R.: Enhanced Depth Imaging Optical Coherence Tomography of Deep Optic Nerve Complex Structures in Glaucoma, Ophthalmology, 119, 2012, 3–9. http://dx.doi.org/10.1016/j.ophtha.2011.07.012

[10] Piegl, L.; Tiller, W.: The NURBS Book, Springer-Verlag, Berlin, 1997. http://dx.doi.org/10.1007/978-3-642-59223-2

[11] Rhodes, L.; Huisingh, C.; Johnstone, J.; Fazio, M.; Smith, B.; Clark, M.; Downs, J.C.; Owsley, C.; Girard, M.J.; Mari, J.M.; Girkin, C.A.: Variation of Laminar Depth in Normal Eyes with Age and Race, Investigative Ophthalmology and Visual Science, 55(12), 2014, 8123–8133. http://dx.doi.org/10.1167/iovs.14-15251

[12] Seo, J.H.; Kim., T.-W.; Weinreb, R.N.: Lamina Cribrosa Depth in Healthy Eyes, Investigative Ophthalmology and Visual Science, 55(3), 2014, 1241–1251. http://dx.doi.org/10.1167/iovs.13-12536

[13] Weinreb, R.N.; Khaw, P.T.: Primary open-angle glaucoma, Lancet, 363, 2004, 1711–1720. http://dx.doi.org/10.1016/S0140-6736(04)16257-0

[14] Wells, A.P.; Garway-Heath, D.F.; Pootschi, A.; Wong, T.; Chan, K.C.Y.; Sachdev, N.: Corneal Hysteresis but not Corneal Thickness Correlates with Optic Nerve Surface Compliance in Glaucoma Patients, Investigative Ophthalmology and Visual Science, 49(8), 2008, 3262–3268. http://dx.doi.org/10.1167/iovs.07-1556